Substrate-Integrated Waveguide Bandpass Filters With Planar Resonators for System-on-Package

Wei Shen, Wen-Yan Yin, *Senior Member, IEEE*, Xiao-Wei Sun, *Member, IEEE*, and Lin-Sheng Wu, *Member, IEEE*

***Abstract*— This paper proposes some novel substrate-integrated waveguide (SIW) bandpass filters combined with planar resonators. According to specific topologies, microstrip lines with different electrical lengths are introduced into their designs. Their corresponding phase-shift characteristics are used to obtain the desired couplings between SIW cavities and the microstrip resonator. Two third-order filter samples are realized. One has a single transmission zero below the passband and the other possesses a quasi-elliptic response. Further, a fourth-order filter is developed by effectively superpositing two individual third-order topologies. It shows better frequency selectivity and flat in-band group delay, with good agreement between the measured and the simulated *S*-parameters. Their compactness and high rejection in the stopbands make them very suitable for system-on-package.**

***Index Terms*— Bandpass filter, dual-mode resonator, quasi-elliptic function, *S*-parameters, substrate-integrated waveguide, system on package, transmission zeros.**

I. Introduction

VARIOUS wireless communication systems require miniaturized radio-frequency (RF) design technologies to satisfy the demands of low cost and compact size. System-in-package (SiP) can provide excellent system integration capabilities with good RF performances by embedding active and passive devices into substrates with low loss [1]. With respect to passive components, the development of bandpass filters is essential for achieving good performance of the system. A well-designed filter should exhibit the desired passband and high rejection level in its stopband. Planar filters, designed using planar structures, possess some advantages such as compact size, low cost, and ease of fabrication. Therefore, they have been widely implemented in the development of many low-power transceiver systems. The designs for conventional microwave filters have been presented in many previous studies [2]–[4]. However, it should be mentioned that the power-handling capacity of conventional planar resonators is always relative low.

On the other hand, it should be pointed out that substrate-integrated waveguides (SIWs) are better candidates for building up SiPs and have attracted much attention recently [5], [6]. They have the advantages of high Q-factor, low loss, high power capacity, and ease of integration with other planar circuits. For example, they have been successfully used for the design of various bandpass filters [7]–[19]. Also, using a multilayered printed circuit board (PCB) as well as low-temperature cofired ceramic (LTCC) technology, SIW components with compact sizes can be realized, as shown in [18] and [19]. Of course, the LTCC fabrication cost is higher than that of single-layered PCB technology.

In this paper, some compact SIW bandpass filters with planar microstrip resonators are proposed. Their coupling schemes are given in Fig. 1(a)–(c). In our design, some planar resonators with different electrical lengths are employed for getting various frequency responses, where the coupling between the SIW cavity and the microstrip resonator is created by certain coplanar waveguide (CPW) structure. Under such circumstances, the configuration of our proposed SIW filter with planar resonator is reduced significantly.

The rest of this paper is organized as follows. Section II describes the required design parameters for realizing the proposed filters. In Section III, coupling coefficients and external Q-factors of the SIW cavity versus physical dimensions are provided. In Section IV, analysis of each filter is carried out, along with its measured S-parameters. Finally, some conclusions are given in Section V.

II. Filter Design

With reference to the coupling schemes shown in Fig. 1(a)–(c), the corresponding configurations of the proposed SIW filters are given in Fig. 2(a)–(c), respectively. Fig. 2(a) shows one third-order SIW filter based on conventional tri-section topology, where microstrip resonators with different

Manuscript received November 13, 2011; revised March 18, 2012; accepted September 17, 2012. Date of publication December 28, 2012; date of current version January 31, 2013. This work was supported in part by the National Basic Research Program under Grant 2009CB320204 and the NSFC of China under Grant 60821062. Recommended for publication by Associate Editor L.-T. Hwang upon evaluation of reviewers' comments.

W. Shen is with the Center for Microwave and RF Technologies, Key Laboratory of Ministry of Education for Design and EMC of High-Speed Electronic Systems, School of Electronic Information and Electrical Engineering, Shanghai Jiao Tong University, Shanghai 200240, China, and also with the Center for Microelectronics, Shanghai Aerospace Research Institute of Electronic Technology, Shanghai 201109, China (e-mail: weishenmw@gmail.com).

W.-Y. Yin is with the Center for Microwave and RF Technologies, Key Laboratory of Ministry of Education for Design and EMC of High-Speed Electronic Systems, School of Electronic Information and Electrical Engineering, Shanghai Jiao Tong University, Shanghai 200240, China, and also with the Center for Optical and Electromagnetic Research, State Key Lab of MOI, Zhejiang University, Hangzhou 310058, China (e-mail: wyyin@zju.edu.cn).

X.-W. Sun is with the Institute of Microsystem and Information Technology, Chinese Academy of Sciences, Shanghai 200050, China.

L.-S. Wu is with the Center for Microwave and RF Technologies, Key Laboratory of Ministry of Education for Design and EMC of High-Speed Electronic Systems, School of Electronic Information and Electrical Engineering, Shanghai Jiao Tong University, Shanghai 200240, China.

Color versions of one or more of the figures in this paper are available online at http://ieeexplore.ieee.org.

Digital Object Identifier 10.1109/TCPMT.2012.2224348

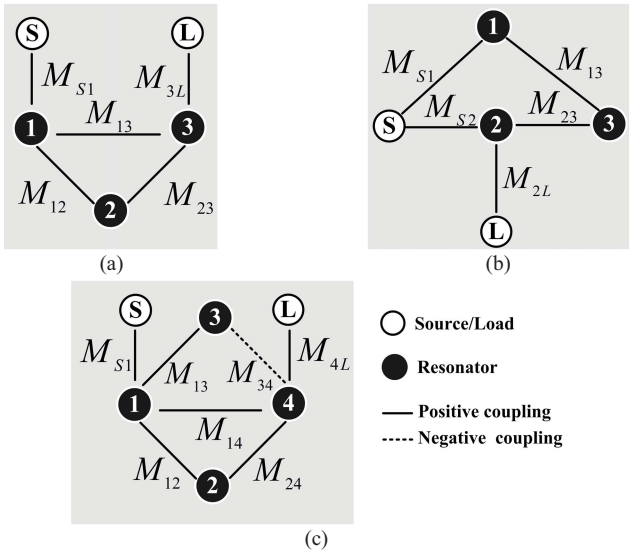

Fig. 1. Coupling scheme of the third-order filter with (a) one transmission zero, (b) quasi-elliptic function, and (c) fourth-order elliptic filter.

electrical lengths are introduced so as to obtain one transmission zero located at its lower or higher stopband.

One novel third-order coupling scheme is presented in Fig. 1(b) which achieves our desired sharp frequency selectivity. The configuration of SIW filter is shown in Fig. 2(b), where one section of the SIW structure is employed to excite both SIW cavities simultaneously, and one microstrip resonator with the length of a single wavelength is used to obtain negative coupling.

Further, one fourth-order coupling scheme, as shown in Fig. 1(c), is also presented, which is the superposition of two third-order ones. Its corresponding SIW configuration with a dual-mode microstrip resonator is given in Fig. 2(c). Both even and odd modes of the microstrip resonator are utilized to achieve positive and negative couplings between the microstrip and the SIW resonators, respectively.

The design parameters of filters, including the coupling coefficients and external Q-factor, the relationship between coupling coefficients, and the physical structure, should be investigated to get the initial dimensions of the filter. The coupling coefficient can be extracted by

$$M_{i,j} = \pm \frac{f_{p2}^2 - f_{p1}^2}{f_{p2}^2 + f_{p1}^2} \tag{1}$$

where f_{p1} and f_{p2} represent the lower and the higher resonant frequencies, respectively. The external Q-factor is given by

$$Q_e = \frac{f_0}{f_{\pm 90^\circ}} \tag{2}$$

where f_0 and $f_{\pm 90}$ denote the central frequency and the $\pm 90^\circ$ bandwidth of the SIW cavity, respectively. Then, the relationship between Q_e and M_{Si} can be described by

$$Q_e = \frac{1}{\mathrm{FBW} \cdot M_{\mathrm{Si}}^2} \tag{3}$$

where FBW represents the designed fractional bandwidth.

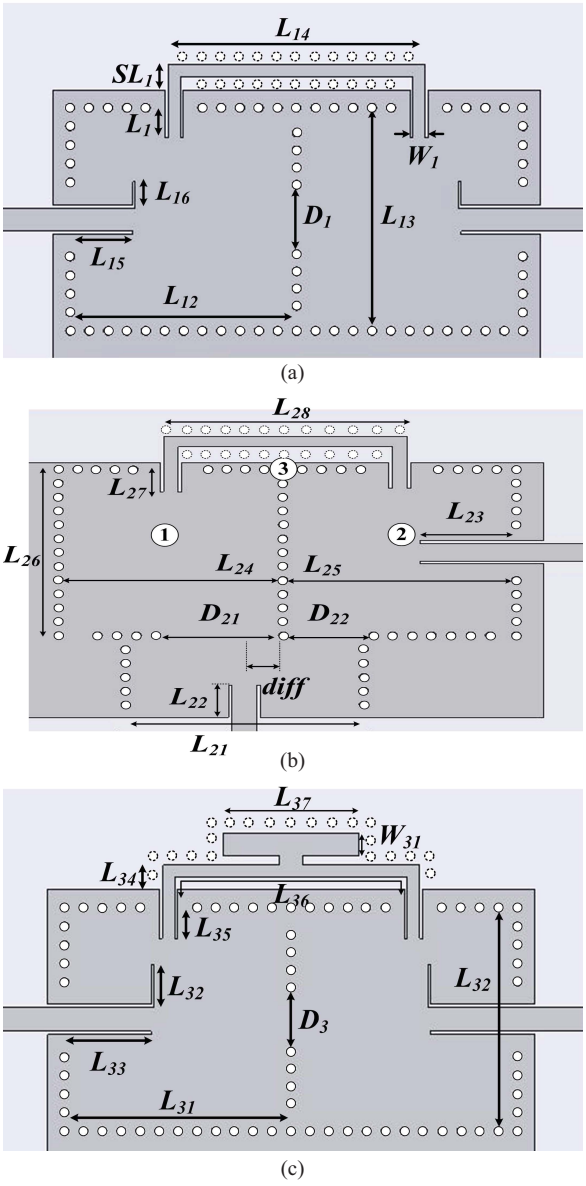

Fig. 2. Top view of the configuration of (a) trisection, (b) modified trisection, and (c) fourth-order SIW filters.

III. Coupling Coefficients and External Q-Factor

A. Coupling Between SIW and Microstrip Resonator

The coupling between the SIW cavity and the microstrip resonator above is realized by the CPW structure, which is etched on the top metal layer. The electric field distributions of TE_{101} mode in the SIW cavity and the quasi-TEM mode in the CPW are plotted in Fig. 3(a) and (b), respectively. It is observed that their electric fields overlap below the strip line, which means that the mode coupling in the structure, integrated by both CPW and SIW, does exist.

As the top metal layer of SIW is grounded by the via holes, the microstrip line is shorted at its two ends. The coupling coefficients between the SIW cavity and the microstrip resonator are plotted in Fig. 4 for different values of D_1 and L_1. It can be seen that the coupling becomes strong as the values of W_1 and L_1 increase. On the other hand, the magnetic coupling

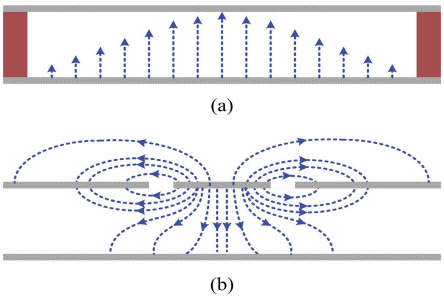

Fig. 3. Electric field distribution of (a) TE_{101} mode in the SIW cavity and (b) quasi-TEM mode in the CPW.

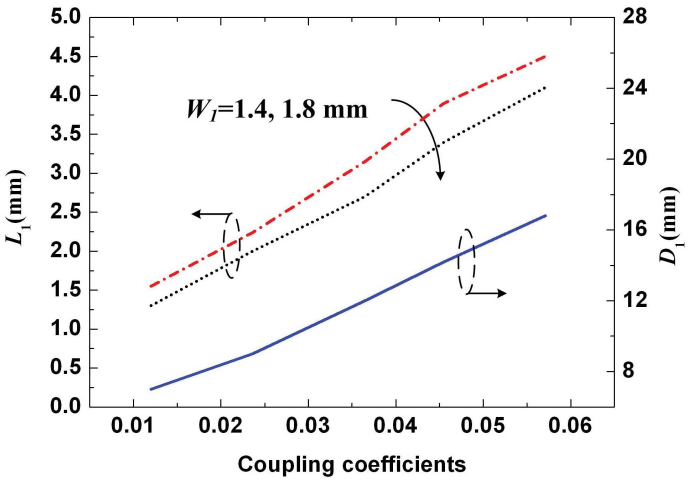

Fig. 4. Coupling coefficient for different values of D_1 and L_1.

between the SIW cavities becomes strong as the value of D_1 increases.

B. External Q-Factor of SIW Cavity

In Fig. 2(a) and (c), the feeding structures are the same. The external Q-factors of SIW cavity are plotted in Fig. 5(a) for different values of L_{15} and L_{16}, which decrease with increasing L_{15} and L_{16}.

Fig. 2(b) shows a novel SIW configuration which is based on one modified trisection in Fig. 1(b). Both external Q-factors of SIW cavities 1 and 2, denoted by Q_e^I and Q_e^{II}, are plotted in Fig. 5(b) and (c) for different values of L_{21}, L_{22}, L_{23}, D_{21}, D_{22}, and diff, respectively. A section of the SIW structure with the width of L_{21} is introduced to excite two SIW cavities simultaneously. The value of L_{21} is large enough so as to make the cut-off frequency below the central frequency. As shown in Fig. 5(c), as L_{21} decreases, the cut-off frequency increases, and Q_e^I becomes larger. In addition, Q_e^I becomes larger with decreasing values of L_{22}, D_{21}, and diff.

IV. Design Examples

A. Analysis of SIW Filters With Microstrip Resonator

Here, our proposed filters are fabricated using a single-layered PCB substrate. Its relative permittivity, loss tangent, and thickness are 2.65, 0.0035, and 1 mm, respectively.

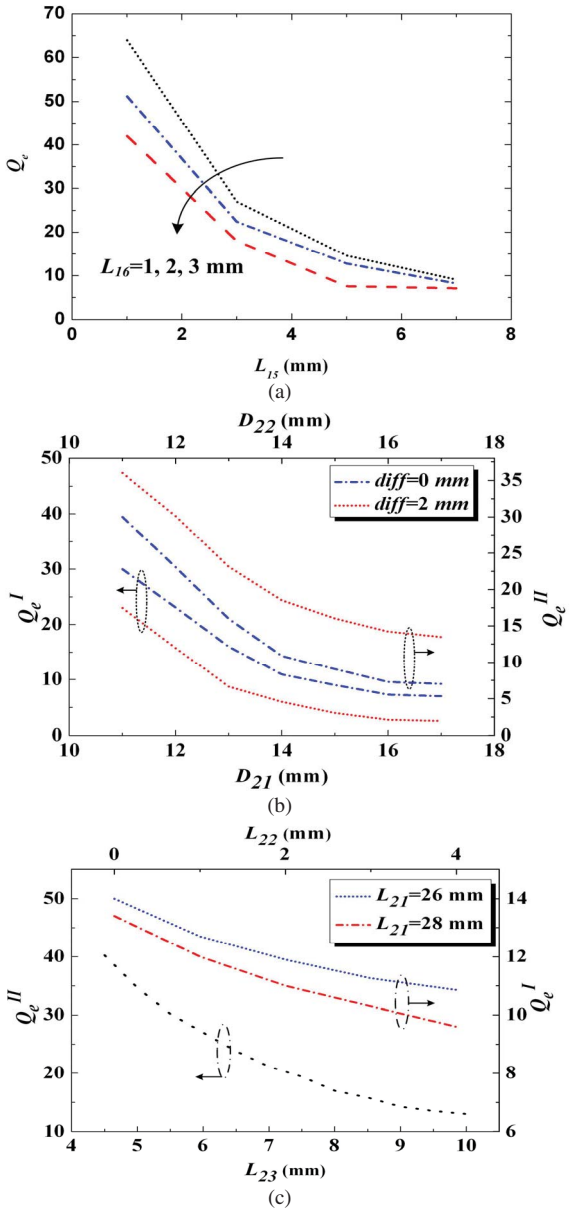

Fig. 5. External Q-factors versus (a) L_{15} and L_{16}, (b) D_{21} and D_{22}, and (c) L_{22} and L_{23}.

The electrical conductivity and thickness of the metal layer are equal to 5.8×10^7 S/m and 0.035 mm, respectively.

For the third-order configuration shown in Fig. 2(a), the second resonator is realized by one microstrip resonator with two shorted ends. One transmission zero can be obtained above the passband. As shown in Fig. 6, a second trisection filter with the first and the third microstrip resonators employed is also presented for comparison. Their simulated S-parameters are also plotted in Fig. 6. It is observed that the insertion losses of the first and second filter are each about 1.4 dB, corresponding to the fractional bandwidths (FBWs) of 4% and 7%, respectively. Obviously, the in-band performance of the second filter is poor in comparison with the first one if same FBWs are obtained. The unloaded Q-factors of microstrip resonators with open ends are lower than those of their counterparts with two shorted ends.

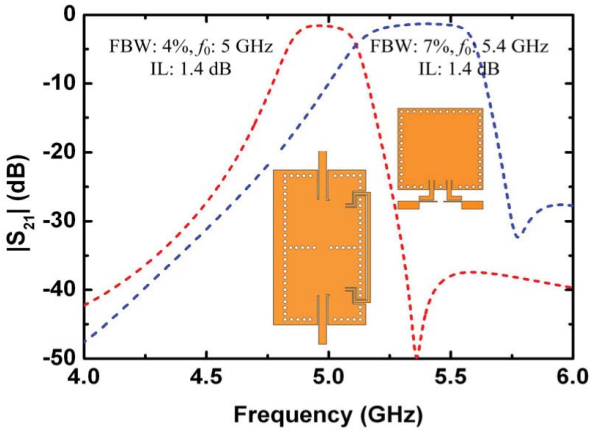

Fig. 6. Simulated S-parameters of different trisection SIW filters with microstrip resonators.

Their corresponding unloaded Q-factors are around 130 and 201, respectively [20], [21].

Meanwhile, the power-handling capacity of the first filter is better. The surface current on the microstrip line gets its maximum at its two ends; the generated heat can be dissipated through the large metal layer area of the SIW cavities. Thus, the presented filters have a higher power-handling capacity in comparison with the classic microstrip ones. Therefore, the implementation of the first filter is taken as primary selection in the system-on-package (SoP).

Then, the unloaded Q-factor of SIW should consist of those of the conductors, the via holes, the dielectric, and the electromagnetic (EM) field leakage

$$\frac{1}{Q_{\text{SIW}}} = \frac{1}{Q_c} + \frac{1}{Q_d} + \frac{1}{Q_{\text{leak}}} = \frac{1}{Q_{\text{metal}}} + \frac{1}{Q_{\text{via}}} + \frac{1}{Q_d} + \frac{1}{Q_{\text{leak}}} \tag{4}$$

$$Q_d = \frac{1}{\tan\delta} \tag{5}$$

$$Q_{\text{metal}} = \frac{h}{\delta_c}, \qquad \delta_c = \frac{1}{\sqrt{\pi f_{\text{TE101}} \mu \sigma_c}} \tag{6}$$

and Q_{via} is calculated by [13]

$$\frac{1}{Q_{\text{via}}} = \frac{2\delta_c}{w}\left(\frac{2p_{\text{via}}}{\pi d_{\text{via}}}\right)^{1.25} \tag{7}$$

where $(2p_{\text{via}}/(\pi d_{\text{via}}))^{1.25}$ is introduced for correcting the lateral currents on the lateral plates that are replaced by the via holes. d_{via} is the diameter of the via hole, and p_{via} is the pitch between them. When $p_{\text{via}} \le 2d_{\text{via}}$, the leakage loss of the structure can be neglected.

The Q-factor of the SIW increases with increase in frequency, and it is 220 at 5 GHz. The Q-factors of SIW cavities are usually higher than those of microstrip lines as the operating frequency increases. Therefore, it should be possible for us to take advantage of the high Q-factor and high power-handling capacity of the SIW structures simultaneously, together with compact size of the microstrip lines.

TABLE I
GEOMETRICAL SIZES OF THE FILTER (UNIT: mm)

Variable	Value	Variable	Value
L_1	3.5	L_{15}	7.1
L_{12}	25.8	L_{16}	3
L_{13}	25.8	SL_1	2.6
L_{14}	29.35	D_1	8

B. Trisection SIW Filter Sample

In order to reduce the filter size, one microstrip resonator of a single wavelength is used to realize the second resonator. Some via holes with dotted lines, as shown in Fig. 2, are introduced to suppress the radiation of the microstrip line.

Fig. 1(a) shows the coupling scheme of the third-order SIW filter with a transmission zero above or below its passband. The S-parameters are determined by [22]

$$S_{11} = 1 + 2j\left[A^{-1}\right]_{1,1} \tag{8a}$$

$$S_{21} = -2j\left[A^{-1}\right]_{N+2,1}. \tag{8b}$$

In order to know how to control the transmission zero, the explicit expression of the transmission zero in a low-pass prototype is provided by

$$\Omega = \frac{M_{12}M_{23}}{M_{13} - M_{22}}. \tag{9}$$

Two points should be indicated as follows.

1) When $\Omega > 0$, direct and cross couplings are the same in nature and, therefore, the transmission zero is located at the upper stopband.
2) When $\Omega < 0$, two direct couplings are different from each other, and the transmission zero is located at the lower stopband.

In (9), $M_{22} \neq 0$ represents the shift from the central frequency of the filter.

The bandwidth and central frequency of the trisection filter, with one transmission zero located at the lower stopband, are set to be 200 MHz and 5 GHz, respectively. At its central frequency f_0, its $(n+2)$ coupling matrix M is given by [22]

$$\boldsymbol{M} = \begin{bmatrix} 0 & 1.081 & 0 & 0 & 0 \\ 1.081 & -0.11 & -0.911 & 0.354 & 0 \\ 0 & -0.911 & 0.295 & 0.911 & 0 \\ 0 & 0.354 & 0.911 & -0.11 & 1.081 \\ 0 & 0 & 0 & 1.081 & 0 \end{bmatrix} \tag{10}$$

and the diagonal elements are determined by

$$M_{i,i} = \frac{f_0^2 - f_i^2}{\Delta f \cdot f_i} \tag{11}$$

where Δf is the filter bandwidth, and f_i is the resonant frequency of the ith resonator.

Further, according to the simulated coupling coefficients and Fig. 4, a set of initial values of L_{15}, L_{16}, D_1, and L_1 are determined. The parameters D_1 and L_1 are used to control the location of transmission zero and bandwidth, respectively.

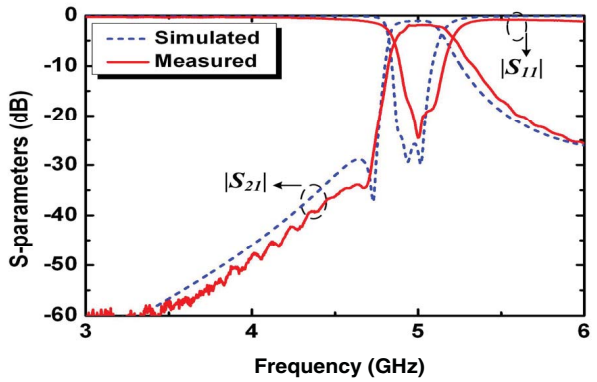

Fig. 7. Simulated and measured S-parameters of the trisection SIW filter as a function of frequency, and its transmission zero below the passband.

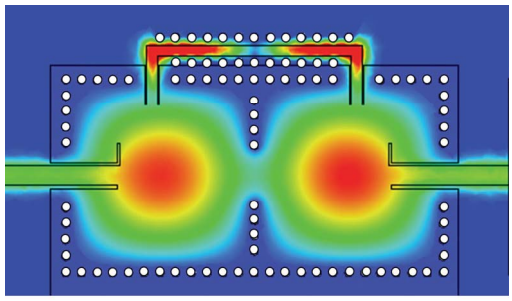

Fig. 8. Electric field distribution of the trisection SIW filter with its transmission zero below the passband.

The geometrical parameter SL_1 is used to adjust the resonant frequency of the microstrip resonator. The whole structure is finely optimized so as to meet our specifications, which is performed using the commercial software high frequency simulator (HFSS).

Its geometrical parameters are summarized in Table I, with its simulated and measured S-parameters plotted in Fig. 7. The filter size is 61 × 32.8 mm, i.e., 1.5 λ_g × 0.97 λ_g, where λ_g is the guided wavelength at its central frequency. Its measured in-band insertion loss is about 1.8 dB, which includes 0.4 dB from two connectors. The passband return loss is better than 18 dB. The measured central frequency and the 3-dB bandwidth are about 5.05 GHz and 210 MHz, respectively. One transmission zero is located at 4.7 GHz, and better than −35 dB rejection at the lower band is observed.

Fig. 8 shows the electric field distribution of the filter at its central frequency. It is seen that there is a 180° phase shift between two SIW cavities, with oppositely directed couplings. It is also observed that the electric field around the microstrip line is confined between two rows of via holes. Its surface current gets its maximum at its two ends and, therefore, its power-handling capacity can be enhanced by integrating it with the SIW cavities.

The presented third-order filter provides one flexible method to move the transmission zero to the lower stopband. It is taken as a type-I filter to make comparisons with the filters given in [7]–[9], such as listed in Table II. Although the above structure is compact, we still need to improve its passband selectivity and spurious suppression. Therefore, one novel third-order coupling scheme is proposed below for further improving the performance of the filter.

TABLE II
COMPARISON WITH THE THIRD-ORDER FILTERS PRESENTED IN REFERENCES

Reference	Size ($\lambda_g \times \lambda_g$)	FBW, f_0 (GHz)	IL (dB)	Number of TZ Below and Above Passband
[7]	1.5 × 1.4	1.6% and 14.6	4	0 and 1
[8]	3.6 × 2.1	5% and 10.0	2.4	1 and 0
[9]	1.5 × 1.4	1.5% and 14.3	2.9	1 and 0
Filter of Type-I	1.5 × 0.97	4% and 5.05	1.8	1 and 0
Filter of Type-II	1.5 × 1.17	4.65% and 5.15	1.47	2 and 2

C. Third-Order Filter With Quasi-Elliptic Function

In order to get better frequency selectivity, one novel coupling scheme with quasi-elliptic function has been shown in Fig. 1(b) and its layout in Fig. 2(b). Based on the topology in Fig. 1(b), the locations of two transmission zeros are determined by

$$\Omega = \frac{\pm[-M_{S2}M_{13} \cdot (M_{S1}M_{23} - M_{S2}M_{13})]^{\frac{1}{2}}}{M_{S2}}. \tag{12}$$

According to (12), the following can be noted.

1) When $M_{13} = M_{23}$, (12) can be simplified as

$$\Omega = \pm M_{13}\left[\frac{-M_{S1}}{M_{S2}+1}\right]^{\frac{1}{2}}. \tag{13}$$

Then, whether $M_{S1} < M_{S2}$, or $M_{S1} > M_{S2}$, Ω is always smaller than unity. Therefore, we cannot get transmission zeros on the imaginary axis of the complex frequency plane.

2) When $M_{13} = -M_{23}$, (12) can be expressed by

$$\Omega = \pm M_{13}\left[\frac{M_{S1}}{M_{S2}+1}\right]^{\frac{1}{2}}. \tag{14}$$

Ω is always larger than unity. Thus, two transmission zeros on the imaginary axis are obtained.

Further, the generalized coupling matrix is obtained and given by

$$\boldsymbol{M}_2 = \begin{bmatrix} 0 & 1.02 & 0.15 & 0 & 0 \\ 1.02 & 0 & 0 & 1.1 & 0 \\ 0.15 & 0 & 0 & -1.1 & 1.2 \\ 0 & 1.1 & -1.1 & 0 & 0 \\ 0 & 0 & 1.2 & 0 & 0 \end{bmatrix}. \tag{15}$$

Here, an SIW section, with width diff, is used to excite two SIW cavities at the same time, which should be large enough to make the filter operate above its cut-off frequency. The parameter diff in Fig. 2(b) is used to control the locations

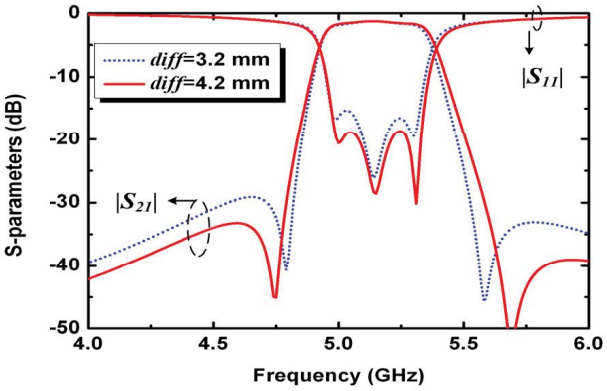

Fig. 9. Simulated S-parameters as a function of frequency for different values of diff.

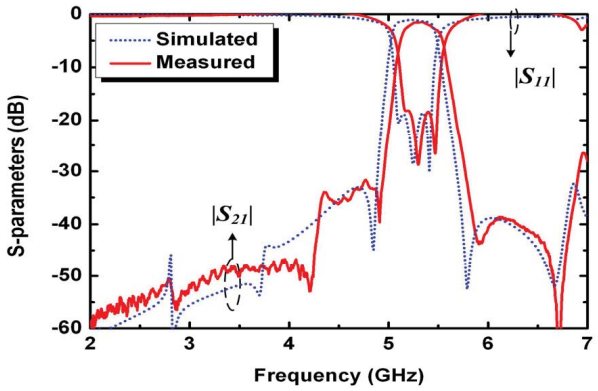

Fig. 10. Simulated and measured S-parameters of the third-order SIW filter in narrow band.

TABLE III
GEOMETRICAL SIZES OF THE FILTER (UNIT: mm)

Variable	Value	Variable	Value
L_{21}	26	L_{26}	25.2
L_{22}	4.9	L_{27}	3.45
L_{23}	10.5	L_{28}	25.8
L_{24}	24.48	D_{21}	13.85
L_{25}	25.44	D_{22}	9.85

of the two transmission zeros. The simulated S-parameters for different cases are plotted in Fig. 9. The term of M_{S1}/M_{S2} in (14) decreases with decreasing diff. Thus, it is found that both transmission zeros shift to the passband as diff decreases.

The geometrical sizes of the fabricated filter are summarized in Table III. Its measured and simulated frequency responses are plotted in Fig. 10, where good agreement has been obtained. Its measured insertion and return losses are around 1.9 and greater than 19 dB, respectively. Its measured central frequency and 3-dB bandwidth are 5.3 GHz and 210 MHz, respectively. Then, additional 0.1–0.2 dB loss is introduced by the SIW section, which is verified by the full-wave EM simulator. Meanwhile, an enhanced passband selectivity is obtained, which is due to the four transmission zeros located at 4.14, 5, 5.9, and 6.75 GHz, respectively. As shown in Fig. 10, the spur appearing around 2.7 GHz is contributing to the first mode in the microstrip resonator. The first and fourth transmission zeros are generated by the coupling between the first and third modes in microstrip resonator and SIW cavities.

As shown in Table II, in comparison with the filters in [7]–[9] our proposed third-order filter is better in frequency selectivity and wider in stopband characteristic.

D. Fourth-Order Filter With Quasi-Elliptic Function

The coupling scheme of the fourth-order filter, as shown in Fig. 1(c), is an appropriate superposition of two trisection topologies. The location of its transmission zero is determined by

$$M_{14}\Omega^2 + \left[M_{13}^2 - M_{12}^2 + M_{14}(M_{22}+M_{33})\right]\Omega \times \left(M_{14}M_{22} - M_{12}^2\right)M_{33} + M_{13}^2 M_{22} = 0. \quad (16)$$

In our design, we set M_{14} as the magnetic (positive) coupling. Therefore, we get the following.

1) When $M_{14} \neq 0$, two transmission zeros are obtained, and they are located at lower and upper stopbands, respectively. Two symmetrical transmission zeros can be obtained when
$$M_{13}^2 - M_{12}^2 + M_{14}(M_{22}+M_{33}) = 0. \quad (17)$$
In general, the term $(M_{22}+M_{33})$ approaches zero, so symmetry is obtained when M_{13} and M_{12} are the same.
2) When $M_{14} = 0$, one transmission zero is located at
$$\Omega = \frac{M_{12}^2 M_{33} - M_{13}^2 M_{22}}{M_{13}^2 - M_{12}^2} \quad (18)$$
and it can be shifted to the lower or the upper stopband by adjusting the coupling coefficients.

The central frequency and bandwidth of the filter are chosen to be 5 GHz and 300 MHz, respectively. Its generalized coupling matrix with cross coupling is given by

$$M = \begin{bmatrix} 0 & 1.18 & 0 & 0 & 0 & 0 \\ 1.18 & 0.029 & 0.697 & 0.75 & 0.21 & 0 \\ 0 & 0.697 & -0.86 & 0 & 0.697 & 0 \\ 0 & 0.75 & 0 & 0.85 & -0.75 & 0 \\ 0 & 0.21 & 0.697 & -0.75 & 0.029 & 1.18 \\ 0 & 0 & 0 & 0 & 1.18 & 0 \end{bmatrix}. \quad (19)$$

Here, we implement a dual-mode resonator with a T-type open stub for the development of the SIW filter. Its layout with two shorted ends is shown in Fig. 11.

Using the odd- and even-mode theory, we can get the resonant frequencies of the odd and even modes as

$$f_n^{\text{odd}} = \frac{c_0 n}{\text{DL}_1\sqrt{\varepsilon_r}} \quad (20a)$$

$$f_n^{\text{even}} = \frac{c_0 n}{\left[\sqrt{\varepsilon_r}\,(2\text{DL}_1 + 2\text{DL}_2 + 4\text{DL}_3)\right]} \quad (20b)$$

where n is the order of resonant mode, and c_0 is the velocity of light in vacuum.

The top view of the proposed SIW filter with dual-mode resonator is shown in Fig. 2(c). The odd mode of microstrip resonator supports a 180° phase difference between two SIW

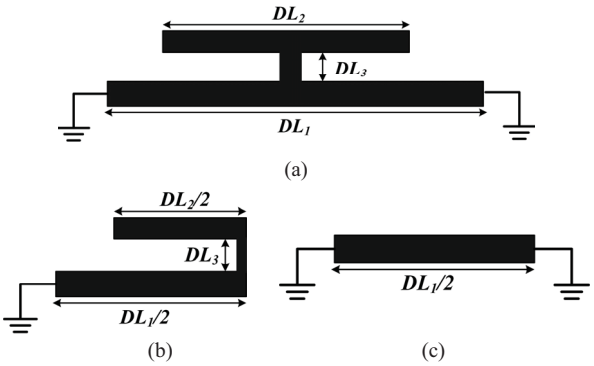

Fig. 11. Layout of (a) dual-mode resonator, and its equivalent (b) even and (c) odd modes.

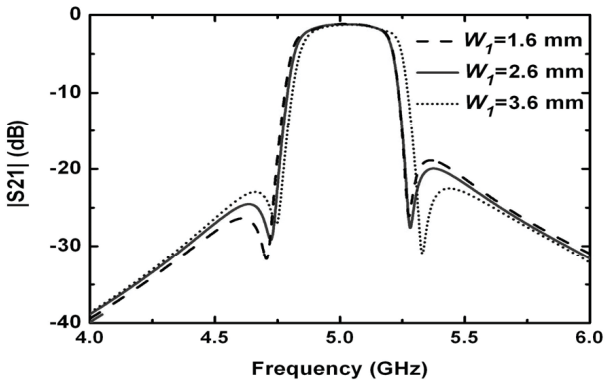

Fig. 12. Simulated S_{21}-parameter as a function of frequency for different values of W_1.

cavities. The coupling between the even mode and two SIW cavities is the same in nature. There is no coupling between the odd and the even modes of the microstrip resonator, and the corresponding coupling scheme given in Fig. 1(c).

As indicated in (16), when the magnitudes of four direct couplings in the upper and lower trisection filters are the same, two transmission zeros are located at the same rejection level. Then, we should find an effective way to control the coupling between the odd or even mode and SIW cavities independently.

The magnetic coupling coefficient is defined by the ratio of the coupled to stored energy

$$k = \frac{\iiint \frac{1}{2}\mu \vec{H}_1 \cdot \vec{H}_2 \mathrm{dv}}{\sqrt{\iiint \frac{1}{2}\mu |\vec{H}_1|^2 \mathrm{dv} \cdot \iiint \frac{1}{2}\mu |\vec{H}_2|^2 \mathrm{dv}}}. \tag{21}$$

Then, the coupling between the resonator 1 and i is calculated by

$$k_{1i} = \frac{\iiint \frac{1}{2}\mu \vec{H}_1 \cdot \vec{H}_2 \mathrm{dv}}{\sqrt{W_1 \cdot W_i}} \tag{22}$$

where W_i represents the stored energy of the ith resonator.

Here, it is assumed that the maximum current on the coupled area between the SIW cavity and the odd or the even mode is the same. Therefore, the ratio of coupling coefficients is obtained by

$$\frac{k_{1o}}{k_{1e}} = \frac{\sqrt{W_e}}{\sqrt{W_o}}. \tag{23}$$

The stored energies of both odd and even modes are calculated by

$$W_o = \int_{-L_{35}-L_{36}/2}^{L_{35}+L_{36}/2} \frac{1}{2} I_0^2 \frac{\cos^2(\beta x) Z_{\mathrm{odd}} \beta}{\omega_0 dx} \tag{24a}$$

$$W_e = \int_{-L_{35}-L_{36}/2}^{L_{35}+L_{36}/2} \frac{1}{2} I_0^2 \frac{\cos^2(\beta x) Z_{\mathrm{odd}} \beta}{\omega_0 dx} + \int_{-L_{37}/2}^{L_{37}/2} \frac{1}{2} I_0^2 \frac{\cos^2(\beta x) Z_{\mathrm{even}} \beta}{\omega_0 dx} \tag{24b}$$

and therefore

$$\frac{k_{1o}}{k_{1e}} = \sqrt{1 + \frac{Z_{\mathrm{even}}}{2Z_{\mathrm{odd}}}}. \tag{25}$$

According to (25), it can be seen that the two couplings between the SIW cavity and the odd or even mode are not equal to each other. According to (16), two symmetrical transmission zeros are obtained when

$$\frac{Z_{\mathrm{even}}}{Z_{\mathrm{odd}}} = \frac{-2M_{14}(M_{22} + M_{33})}{M_{12}^2}. \tag{26}$$

We know that the four direct couplings are sensitive to the variation of parameter L_5. Here, W_1 is used to control the coupling between the even mode and the SIW cavity independently. Z_{even} becomes smaller with increase in the value of W_1, and therefore k_{1o}/k_{1e} becomes small. Finally, we can get two symmetrical transmission zeros just by changing W_1.

As explained above, the parameter L_{35} is used to adjust the filter bandwidth, and the locations of two transmission zeros are controlled by D_3 simultaneously. The simulated S-parameters of the filter are plotted in Fig. 12 for different values of W_{31}. The coupling between the even mode and the SIW cavity becomes strong with increasing values of W_{31}, so the transmission zeros located at the upper and lower stopbands move far from and close to the passband, respectively. Therefore, two transmission zeros can get the same level of rejection just by tuning W_{31}.

The geometrical parameters of the fourth-order filter, as illustrated in Fig. 2(c), are summarized in Table IV, and its simulated and measured S-parameters plotted in Fig. 13. The measured insertion loss is about 2.05 dB, which is larger than the simulated one of 1.5 dB. The difference is because the measured bandwidth is 210 MHz, which is smaller than 280 MHz of its counterpart. It is almost flat around the central frequency and the variation in the passband of our measured results is about 0.2 ns.

TABLE IV
GEOMETRICAL SIZES OF THE FILTER (UNIT: mm)

Variable	Value	Variable	Value
L_{35}	3.6	L_{36}	29.35
L_{32}	5	L_{37}	15.45
L_{33}	9.9	L_{31}	25.8
L_{34}	5	L_{32}	25.8
W_{31}	2.6	D_3	7.4

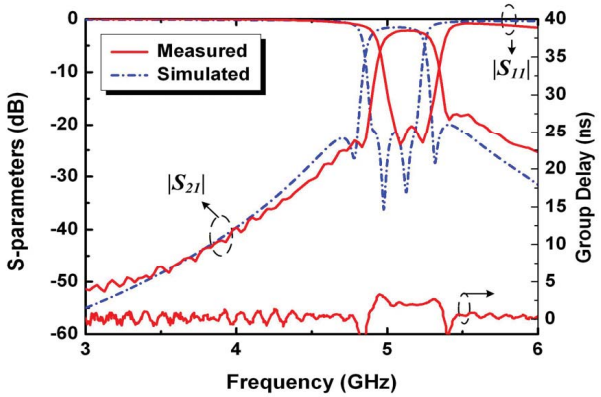

Fig. 13. Simulated and measured S-parameter and group delay of the fourth-order SIW filter as a function of frequency.

TABLE V
COMPARISON WITH THE THIRD-ORDER FILTERS PRESENTED IN REFERENCES

Reference	Size ($\lambda_g \times \lambda_g$)	FBW, f_0 (GHz)	IL (dB)	TZs Below and Above Passband
[12]	1.6 × 1.42	4.4% and 20.5	0.9	1 and 1
[17]	2.9 × 1.4	2% and 10.0	2.6	1 and 1
This paper	1.55 × 0.98	4.2% and 5.1	2.05	1 and 1

Finally, as listed in Table V, we make some comparisons between the proposed fourth-order filter and the previous planar ones in [12] and [17]. Our presented filter is reduced in size by 40%, and they have relatively flat in-band group delay.

V. CONCLUSION

In this paper, we presented some novel SIW bandpass filters realized using certain topologies. For the purpose of miniaturization, microstrip lines with different electrical lengths were used to replace the SIW cavity. In our designs, a one-wavelength microstrip line was introduced into the trisection SIW filter, and then one transmission zero was obtained below its passband. Furthermore, a novel third-order coupling scheme was presented, and the filter sample had better frequency selectivity and wider stopband. Finally, a dual-mode microstrip resonator was implemented in the development of a fourth-order SIW filter, with quasi-elliptic function as well as flat group delay in their passbands, respectively. All of them had high rejection level in the stopband. In our design, the surface current on the microstrip line gets its maximum at its two ends; the generated heat can be dissipated through large metal layer area of the SIW cavities. Thus, the presented filters have higher power-handling capacity in comparison with the classic microstrip ones. Meanwhile, our proposed filters, in comparison with the planar SIW ones, can also achieve 40% size reduction. Therefore, the proposed structures are suitable for the development of some SoPs.

REFERENCES

[1] R. R. Tummala and M. Swaminathan, *Introduction to System-on-Package (SOP)*. New York: McGraw-Hill, 2008.
[2] J. S. Hong and M. J. Lancaster, *Microstrip Filters for RF/Microwave Applications*. New York: Wiley, 2001.
[3] R. J. Cameron, C. M. Kudsia, and R. R. Mansour, *Microwave Filters for Communication Systems: Fundamentals, Desing, and Applications*. New York: Wiley, 2007.
[4] G. L. Mattaei, E. M. T. Jones, and L. Young, *Microwave Filters, Impedance-Matching Network, and Coupling Structures*. Norwood, MA: Artech House, 1964, chs. 8–12.
[5] A. J. Piloto, K. A. Leahy, B. A. Flanick, and K. A. Zaki, "Waveguide filters having a layered dielectric structures," U.S. Patent 5 382 931, Jan. 13, 1995.
[6] Y. J. Chen, K. Wu, and W. Hong, "Power handing capability of substrate integrated waveguide interconnects and related transmission line system," *IEEE Trans. Antennas Propag.*, vol. 31, no. 4, pp. 900–909, Nov. 2008.
[7] B. Potelon, J.-C. Bohorquez, J.-F. Favennec, C. Quendo, E. Rius, and C. Person, "Design of Ku band filters based on substrate integrated circular cavities (SICCs)," in *IEEE MTT-S Int. Micro. Symp. Dig.*, Jun. 2006, pp. 1237–1240.
[8] Q. F. Wei, Z. F. Li, W. J. Zhang, and J. F. Mao, "Three-pole cross-coupled substrate integrated waveguide (SIW) bandpass filters based on PCB process and multilayer LTCC technology," *Microw. Opt. Technol. Lett.*, vol. 51, no. 1, pp. 71–73, Jan. 2009.
[9] B. Potelon, J.-F. Favennec, C. Quendo, E. Rius, C. Person, and J.-C. Bohorquez, "Design of a substrate integrated waveguide (SIW) filter using a novel topology of coupling," *IEEE Microw. Wireless Compon. Lett.*, vol. 18, no. 9, pp. 956–958, Sep. 2008.
[10] W. Shen, L. S. Wu, X. W. Sun, W. Y. Yin, and J. F. Mao, "Novel substrate integrated waveguide filters with mixed cross coupling," *IEEE Microw. Wireless Compon. Lett.*, vol. 19, no. 11, pp. 701–703, Nov. 2009.
[11] C. Y. Chang, and W.-C. Hsu, "Novel planar, square-shaped, dielectric-waveguide, single-, and dual-mode filters," *IEEE Trans. Microw. Theory Tech.*, vol. 50, no. 11, pp. 2527–2536, Nov. 2002.
[12] X. P. Chen and K. Wu, "Substrate integrated waveguide cross-coupled filter with negative coupling structure," *IEEE Trans. Microw. Theroy Tech.*, vol. 56, no. 1, pp. 142–149, Jan. 2008.
[13] L. S. Wu, L. Zhou, X. L. Zhou, and W. Y. Yin, "Bandpass filter using substrate integrated waveguide cavity loaded with dielectric rod," *IEEE Microw. Wireless Compon. Lett.*, vol. 19, no. 8, pp. 491–493, Aug. 2009.
[14] L. S. Wu, X. L. Zhou, Q. F. Wei, and W. Y. Yin, "An extended doublet substrate integrated waveguide (SIW) bandpass filter with a complementary split ring resonator (CSRR)," *IEEE Microw. Wireless Compon. Lett.*, vol. 19, no. 12, pp. 777–779, Dec. 2009.
[15] W. Shen, X. W. Sun, W. Y. Yin, J. F. Mao, and Q. F. Wei, "A novel single-cavity dual node substrate integrated waveguide filter with non resonating node," *IEEE Microw. Wireless Compon. Lett.*, vol. 19, no. 6, pp. 368–370, Jun. 2009.
[16] J. S. Hong and M. J. Lancaster, "Transmission line filters with advanced filtering characteristics," in *IEEE MTT-S Int. Micro. Symp. Dig.*, vol. 1. Aug. 2000, pp. 319–322.
[17] X. P. Chen, W. Hong, T. J. Cui, Z. C. Hao, and K. Wu, "Substrate integrated waveguide elliptic filter with transmission line inserted inverter," *Electron. Lett.*, vol. 41, no. 15, pp. 851–852, Jul. 2005.
[18] T. M. Shen, C. F. Chen, T. Y. Huang, and R. B. Wu, "Design of vertically stacked waveguide filters in LTCC," *IEEE Trans. Microw. Theory Tech.*, vol. 55, no. 8, pp. 1771–1779, Aug. 2007.
[19] L. S. Wu, X. L. Zhou, W. Y. Yin, L. Zhou, and J. F. Mao, "A substrate integrated evanescent-mode waveguide filter with nonresonating node in low-temperature co-fired ceramic," *IEEE Trans. Microw. Theory Tech.*, vol. 58, no. 10, pp. 2654–2662, Oct. 2010.
[20] K. C. Gupta, R. Garg, I. Bahl, and P. Bhartia, *Microstrip Lines and Slotlines*. Norwood, MA: Artech House, 1996.
[21] L. Lewin, "Radiation from discontinuities in strip-line," *Proc. Inst. Electr. Eng.*, vol. 107, no. 12, pp. 163–170, Feb. 1960.
[22] S. Amari, U. Rosenberg, and J. Bornemann, "Adaptive synthesis and design of resonator filters with source/load-multi-resonator coupling," *IEEE Trans. Microw. Theory Tech.*, vol. 50, no. 8, pp. 1969–1978, Aug. 2002.

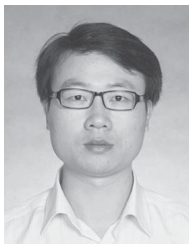

Wei Shen was born in Anhui, China, in 1981. He received the B.Eng. and M.Eng. degrees from the University of Anhui, Hefei, China, in 2004 and 2007, respectively, and the Ph.D. degree from Shanghai Jiao Tong University, Shanghai, China, in 2012.

He is currently an Engineer with Shanghai Aerospace Research Institute of Electronic Technology, Shanghai. His current research interests include passive RF and microwave circuits, and filters for wireless applications and systems on package.

Wen-Yan Yin (M'99–SM'01) received the M.Sc. degree in electromagnetic fields and microwave techniques from Xidian University, Xi'an, China, and the Ph.D. degree in electrical engineering from Xi'an Jiao Tong University, Xi'an, in 1989 and 1994, respectively.

He was an Associate Professor with the Department of Electronic Engineering, Northwestern Polytechnic University, Xi'an, from 1993 to 1996. He was a Research Fellow with the Department of Electrical Engineering, Duisburg University, Duisburg, Germany, from 1996 to 1998, granted by the Alexander von Humboldt-Stiftung, Bonn, Germany. He has been with Department of Electrical Engineering, National University of Singapore (NUS), Singapore, as a Research Fellow, since 1998, where he joined the Temasek Laboratories in 2002, as a Research Scientist and a Project Leader. Since 2005, he has been a Professor with the School of Electronic Information and Electrical Engineering, Shanghai Jiao Tong University, Shanghai, China. He joined the National State Key Laboratory of Modern Optical Instrumentation, Zhejiang University, Hangzhou, China, as a "Qiu Shi" Chair Professor, in 2009. He has authored or co-authored over 190 international journal papers, one international book, and 17 book chapters. His current research interests include passive and active RF and millimeter-wave device and circuit modeling, ultrawideband interconnects and signal integrity, nanoelectronics, electromagnetic compatibility and electromagnetic protection, and computational multiphysics and applications. Dr. Yin was a recipient of the Best Paper Award of the 2008 Asia–Pacific Symposium on Electromagnetic Compatibility and the 19th International Zurich Symposium, Singapore. He is an IEEE EMC Society Distinguished Lecturer from 2011 to 2012.

Xiao-Wei Sun (A'04–M'05) was born in Beijing, China, in 1958. She received the B.S., M.S., and Ph.D. degrees in electrical engineering from Xi'an Jiaotong University, Xi'an, China, in 1982, 1984, and 1996, respectively.

She joined the Institute of Microsystems and Information Technology, Chinese Academy of Sciences, Singapore, in 1997, where she is currently a Professor and the Director of the Laboratory of RF and Microsystem Technology. Her current research interests include microwave and millimeter-wave devices and monolithic microwave integrated circuits design, process, and measurement.

Lin-Sheng Wu (S'09–M'10) received the B.S. degree in electronic engineering and the M.S. and Ph.D. degrees in electromagnetic fields and microwave techniques from Shanghai Jiao Tong University (SJTU), Shanghai, China, in 2003, 2006, and 2010, respectively.

He is currently a Post-Doctoral Researcher with the Center for Microwave and RF Technologies, Department of Electronic Engineering, SJTU. He is a Research Fellow with the Department of Electrical and Computer Engineering, National University of Singapore, Singapore, in 2010. His current research interests include novel techniques for microwave integration, microwave and RF components, hybrid electrothermal problems for systems-on-package, intelligent information processing, and passive localization.